Silica-Sulfonated Iron Oxide Hybrid for Superior Methylene Blue Degradation

Maria Ulfa[1*], and *Pramesta Rosa* Salsabilaa[1]

[1]Chemistry Education Study Program, Faculty of Teacher Training and Education, Sebelas Maret University, Jl. Ir. Sutami 36A, Surakarta 57126, Indonesia

Abstract. This study presents the synthesis and photocatalytic performance of SSIO (silica-sulfonated iron oxide) for the degradation of methylene blue, directly comparing it with pure iron oxide (IO). The SSIO catalyst was prepared via a soft-template approach using gelatin and P123, followed by sulfonation and Fe_2O_3 incorporation through wet impregnation, resulting in a pale-yellow, fine powder.XRD analysis confirmed Fe_2O_3 crystallites in SSIO with an average size of 2.08 nm and crystallinity of 89.2%, while FTIR spectra indicated –COOH, Si–OH, and Si–O–Si groups. Sulfonic acid-related signals were not clearly observed in the XRD, suggesting a predominantly amorphous or low-crystallinity nature. SEM imaging showed short rod- and platelet-like structures, providing a high surface area for catalytic reactions.Photocatalytic tests revealed that SSIO degraded methylene blue with an efficiency of 88.7% within 90 minutes, significantly higher than IO, which achieved 72.5% under the same conditions. Kinetic analysis followed a pseudo-first-order model with a rate constant of 0.0135 min^{-1} for SSIO. These results demonstrate that incorporating sulfonated silica into SSIO substantially enhances photocatalytic activity compared to IO alone, offering a low-cost and efficient solution for treating dye-contaminated wastewater.

1 Introduction

The rapid industrial development in Indonesia, under the “Making Indonesia 4.0” initiative, has significantly advanced the manufacturing sector, particularly in textiles, which contribute to both domestic and global markets [1]. While this growth supports economic development, it also generates environmental challenges, notably the release of wastewater laden with dyes. Methylene Blue (MB), a widely used cationic dye ($C_{16}H_{18}ClN_3S$), is highly soluble, intensely coloured, and resistant to conventional degradation processes, posing a threat to aquatic ecosystems by reducing sunlight penetration and dissolved oxygen [2-4].

Traditional treatment methods, including chlorination , ozonation, and biodegradation, are often insufficient or economically unfeasible in developing countries [5]–[7]. Even adsorption techniques may leave residual organic pollutants, leading to secondary contamination [8]. Photocatalysis has emerged as a promising solution, leveraging semiconductor materials activated by light to generate reactive species that can degrade

* Corresponding author: mariaulfa@staff.uns.ac.id

persistent organic pollutants [9]–[10]. Among metal oxides, Fe_2O_3 is attractive due to its visible-light activity, low toxicity, and cost-effectiveness [11]–[12]. However, many Fe_2O_3-supported catalysts face limitations such as low surface area, poor dispersion, or inefficient interaction with target pollutants.

In this study, a novel mesoporous hybrid material, SSIO (silica-sulfonated iron oxide), was developed by incorporating Fe_2O_3 nanoparticles into sulfonated mesoporous silica synthesised using P123 and gelatin as dual soft templates. The sulfonated silica framework not only improves the dispersion of Fe_2O_3 but also enhances adsorption and photocatalytic performance. The structural and functional properties of SSIO were characterized using X-ray diffraction (XRD), Fourier-transform infrared spectroscopy (FTIR), and UV-Vis spectroscopy, and its photocatalytic activity was evaluated in the degradation of methylene blue. By combining sulfonation with Fe_2O_3 impregnation, SSIO addresses critical limitations of conventional Fe_2O_3 catalysts while offering a low-cost, environmentally friendly solution to persistent dye pollution—a global water quality concern [1]–[9].

2 Materials and Methods

2.1 Materials

The chemicals used in this study include hydrochloric acid (HCl, 37%, Sigma-Aldrich, Mr 36.5 g/mol), distilled water (Smart-Lab, Mr 18 g/mol), poly(ethylene oxide)-block-poly(propylene oxide)-block-poly(ethylene oxide) surfactant $EO_{106}PO_{70}EO_{106}$ (Sigma-Aldrich, Mr 5750 g/mol), commercial gelatin (Gelita, Mr ≈90,000 g/mol), tetraethoxysilane ($Si(OC_2H_5)_4$, Sigma-Aldrich, Mr 208.33 g/mol), methylene blue dye (Sigma-Aldrich), and iron(III) chloride hexahydrate ($FeCl_3 \cdot 6H_2O$, Sigma-Aldrich).

2.2 Synthesis and sulfonation of gelatin-modified mesoporous silica (SS)

Gelatin-modified mesoporous silica was synthesized by dissolving poly(ethylene oxide)-block-poly(propylene oxide)-block-poly(ethylene oxide) ($EO_{106}PO_{70}EO_{106}$) and gelatin in diluted hydrochloric acid at a mass ratio of 5:1. The surfactant mixture was dissolved in HCl using a molar ratio of 1.0 HCl : 0.8 $EO_{106}PO_{70}EO_{106}$ and stirred at 40 °C for 3 h. Tetraethoxysilane ($Si(OC_2H_5)_4$) was then added with a feed molar ratio of 3.5 $Si(OC_2H_5)_4$: ($EO_{106}PO_{70}EO_{106}$ + gelatin). The mixture was stirred for 24 hours and then subjected to hydrothermal treatment at 90 °C for an additional 24 hours. The solid product was filtered, washed, dried, and calcined at 550 °C to obtain gelatin-modified mesoporous silica. The resulting material was activated in 0.1 M hydrochloric acid using a solid-to-solution ratio of 1:50 for 24 hours, followed by filtration, washing, and drying. Sulfonation was carried out by reacting the activated silica with concentrated sulfuric acid at a solid : acid ratio of 1 : 10 (mL g^{-1}) for 20 h under reflux. The sulfonated material was washed with hot water and denoted as SS.

2.3 Synthesis sulfonation of mesoporous silica iron oxide (SSIO)

Iron oxide was incorporated into SS using a 10 mol% Fe^{3+} : SiO_2 ratio. $FeCl_3 \cdot 6H_2O$ was dissolved in distilled water (1 60 Fe^{3+} : H_2O molar ratio) and mixed with SS (1 9 Fe^{3+} : SS mass ratio). The mixture was stirred at 45 °C for 16 h, dried, washed and calcined at 450 °C to obtain SSIO.

2.4 Synthesis of pure iron oxide (IO)

Pure iron oxide (IO) was prepared by dissolving $FeCl_3 \cdot 6H_2O$ in distilled water using a 1 100 Fe^{3+} : H_2O molar ratio. The solution was allowed to precipitate, followed by centrifugation, filtration, drying at 120 °C for 12 h, and calcination at 450 °C for 4 h.

2.5 Photocatalytic degradation of methylene blue

Photocatalytic activity was evaluated using 50 mg of catalyst (SSIO or IO) dispersed in 200 mL of 5 ppm methylene blue solution, corresponding to a catalyst-to-dye molar ratio of approximately 1 : 28 (Fe : MB). Prior to irradiation, the suspension was kept in the dark for 30 min to reach adsorption–desorption equilibrium. The system was then exposed to UV light under constant stirring, and 10 mL aliquots were withdrawn at predetermined time intervals (0–90 min). A control sample was collected at t = 0 (without light exposure), and all photocatalytic experiments were conducted in triplicate to ensure reproducibility**.** The concentrations of methylene blue were quantified spectrophotometrically at 665 nm using a UV–Vis spectrophotometer.

3 Results and Discussion

3.1 X-Ray Diffraction (XRD) analysis

Figure 1 shows the XRD diffraction patterns of IO (iron oxide), SS (gelatin-templated mesoporous silica that has been sulfonated), and SSIO (sulfonated silica impregnated with iron oxide). The IO sample displays several sharp and intense diffraction peaks, indicating a high degree of crystallinity and the characteristic reflections of crystalline Fe_2O_3. In contrast, the SS sample exhibits a broad and low-intensity pattern, confirming its amorphous silica nature after gelatin templating and sulfonation. When Fe_2O_3 is incorporated into the sulfonated silica framework (SSIO), a combination of features from both IO and SS is observed. Specifically, the diffraction profile of SSIO exhibits a broad amorphous background of silica, accompanied by several distinct peaks attributable to crystalline Fe_2O_3, which confirms the successful impregnation of iron oxide into the sulfonated silica matrix. The presence of these Fe_2O_3 reflections in SSIO also indicates that the iron oxide particles maintain their crystalline structure after incorporation.

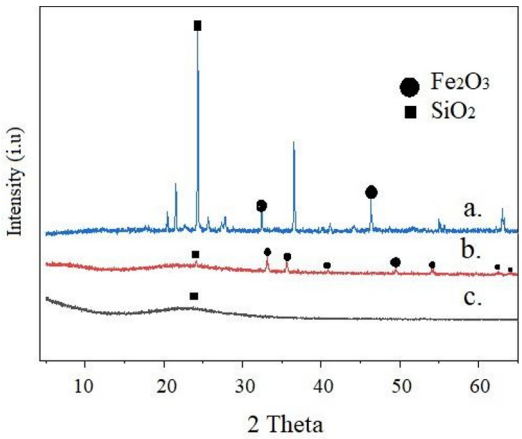

Fig. 1. XRD of a. IO, b. SSIO and C. SS sample.

In addition to the qualitative identification of crystalline phases, the diffraction patterns also reveal differences in crystallinity and possible structural interactions among the samples. The IO sample exhibits narrow and high-intensity peaks at 2θ values of approximately 24.1°, 33.2°, 35.6°, and 49.5°, corresponding to the (012), (104), (110), and (024) planes of α-Fe_2O_3, respectively, indicating well-defined crystalline domains. For the SS sample, the absence of sharp reflections and the presence of a broad halo centered around 22° confirm the amorphous nature of the mesoporous silica after gelatin templating and sulfonation. This feature is typically associated with short-range Si–O–Si ordering without any long-range crystallinity.

In the case of SSIO, the XRD pattern presents a combination of broad background from the silica matrix and several distinct peaks located at similar 2θ positions to those observed in IO. However, these peaks are slightly broadened and exhibit a minor shift toward lower 2θ values compared to pure IO. The peak broadening indicates a reduction in crystallite size due to the dispersion of Fe_2O_3 nanoparticles on the silica surface, while the slight shift suggests the occurrence of interfacial interactions between the iron oxide phase and sulfonated silica matrix. Such interactions can generate lattice strain or partial incorporation of Fe–O–Si bonds , which consequently alter the local structure and cause marginal 2θ displacement. Overall, the diffraction data demonstrate that Fe_2O_3 retains its crystalline structure after impregnation, while its crystallite size and lattice parameters are affected by the dispersion within the sulfonated silica framework. This confirms the successful formation of a hybrid SSIO material with intimate contact between the metal oxide and functionalized mesoporous silica.The crystallite size of the Fe_2O_3 phase was estimated using the Scherrer equation [13]:

$$D = K\lambda / (\beta \cos \theta)$$

where D is the crystallite size, K is the shape factor (taken as 0.9), λ is the X-ray wavelength (0.15406 nm for Cu Kα), β is the full width at half maximum (FWHM) of the selected diffraction peak (in radians), and θ is the Bragg angle. The (104) reflection of α-Fe_2O_3 was selected for the calculation. The calculated crystallite size of pure iron oxide was approximately 2.14 nm, while the SSIO sample exhibited a slightly smaller value of 2.08 nm. This reduction in crystallite size further supports the hypothesis that Fe_2O_3 is highly dispersed on the sulfonated silica surface and interacts with the support, which restricts particle growth during calcination.

3.2 Fourier Transform Infrared (FTIR) spectroscopy

Figure 2 presents the FTIR spectra of IO (iron oxide), SSIO (sulfonated silica impregnated with iron oxide), and SS (sulfonated gelatin-templated silica). The spectrum of the SS sample (curve c) exhibits broad absorption bands at 3388–3370 cm^{-1}, which correspond to the stretching vibration of surface –OH groups originating from silanol and adsorbed water [14]. The band at approximately 1632 cm^{-1} is assigned to the bending vibration of molecular water. The characteristic silica framework bands can be observed at 1054–1065 cm^{-1} (asymmetric Si–O–Si stretching), 799 cm^{-1} (symmetric Si–O–Si stretching), and 444–448 cm^{-1} (Si–O bending), confirming the formation of mesoporous silica after gelatin templating and sulfonation [15]. The IO sample (curve a) displays a strong absorption band at around 530–531 cm^{-1}, which is characteristic of the Fe–O stretching mode in crystalline Fe_2O_3. The absence of silica-related bands in this spectrum confirms that the material consists solely of iron oxide.

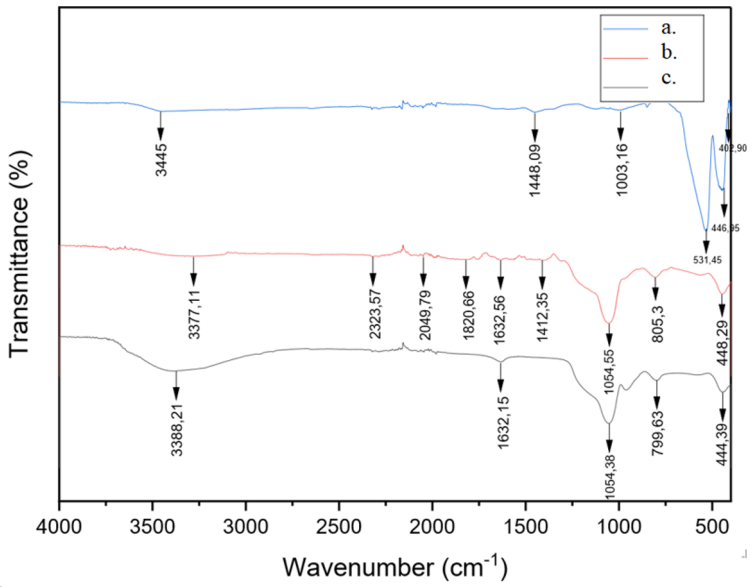

Fig. 2. FTIR of a. IO, b. SSIO and C. SS sample.

For the SSIO sample (curve b), the FTIR spectrum shows a combination of both silica- and iron oxide–related bands. The broad –OH stretching band remains observable at ~3377 cm^{-1}, indicating that surface silanols are still present after impregnation. The Si–O–Si stretching band at 1054 cm^{-1} is slightly shifted and decreased in intensity compared to pure SS, suggesting an interaction between the Fe_2O_3 phase and the functionalized silica surface. Additionally, the Fe–O absorption band appears at approximately 531 cm^{-1}, confirming the successful incorporation of iron oxide into the sulfonated silica matrix. The absence of a distinct peak corresponding to $–SO_3H$ (typically at ~1230 cm^{-1}) indicates that sulfonic groups are dispersed in an amorphous or weakly bonded state. Overall, the FTIR spectra demonstrate the presence of Si–O–Si and Fe–O bonds in the hybrid SSIO material, confirming that the impregnation process does not destroy the functional groups of the sulfonated silica but rather allows for interaction between the two phases.

3.3 SEM

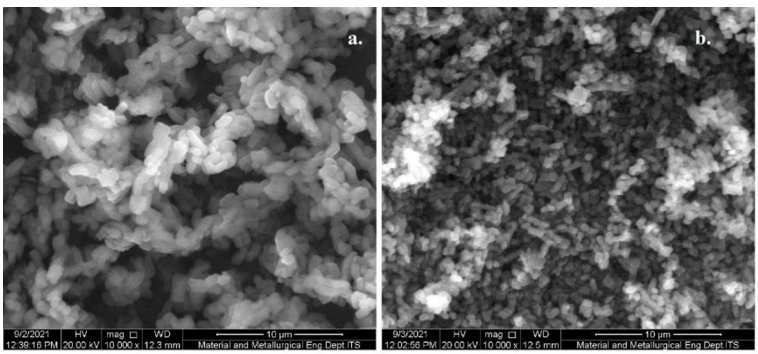

Fig. 3. SEM of a. SS and SSIO sample.

The photodegradation performance of the synthesized catalysts was evaluated by monitoring the removal efficiency of the dye as a function of irradiation time (Figure 4). In general, both catalysts exhibited a rapid increase in photodegradation activity within the first 30 min, corresponding to the rapid generation of reactive oxygen species and the adsorption–photocatalysis synergetic effect. However, a clear difference in performance can be observed between the SSIO and IO samples. The SSIO catalyst (a) exhibited a significantly higher photodegradation efficiency throughout the entire experiment, reaching a maximum efficiency of ~88.7% after 40 minutes of irradiation and remaining nearly constant thereafter. This enhanced activity can be attributed to the strong interaction between the sulfonated silica support and the Fe_2O_3 nanoparticles, which improves light harvesting, charge separation efficiency, and surface accessibility for the dye molecules.

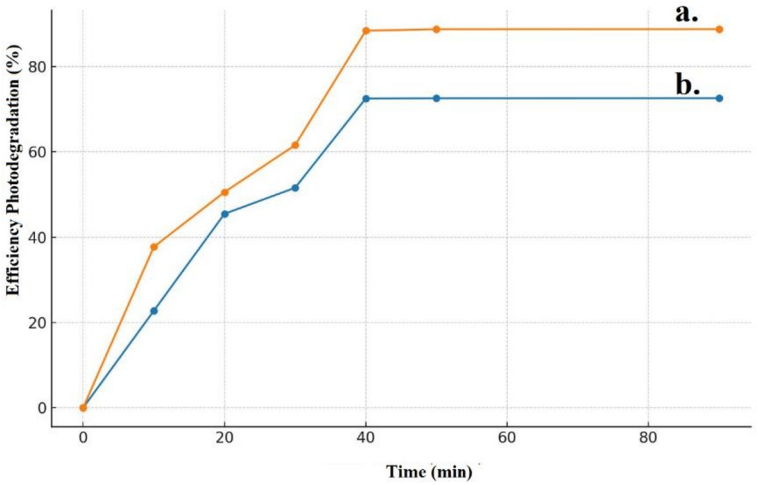

Fig. 3. Photodegradation performance of a. SSIO and SS sample.

In other side, the IO catalyst (b) only achieved ~72.5% degradation under similar conditions and exhibited a slower rate of activity enhancement. The lower efficiency could be associated with the rapid recombination of photogenerated electron–hole pairs and the limited surface area of pristine Fe_2O_3. These observations clearly demonstrate the beneficial role of the sulfonated silica framework in enhancing the photocatalytic performance of iron oxide via improved dispersion and surface functionalization.The kinetic behaviour of dye photodegradation was evaluated using both pseudo-first-order and pseudo-second-order models, with the normalised concentration (C/C_0) plotted as a function of time. As shown in Figure 4, the SSIO sample exhibited a faster degradation rate with a pseudo-first-order rate constant of 0.0135 min^{-1}, compared to 0.008 min^{-1} for IO. The sharper decline in C/C_0 for SSIO confirms its superior photocatalytic activity due to the synergistic effect of sulfonated silica support and well-dispersed iron oxide species.

Table 1. Kinetic parameters of SSIO and IO.

Model	Sample	Rate constant (min^{-1})	R^2
Pseudo-first-order	SSIO	0.0135	0.98
Pseudo-first-order	IO	0.0080	0.95
Pseudo-second-order	SSIO	0.0010	0.92
Pseudo-second-order	IO	0.0006	0.88

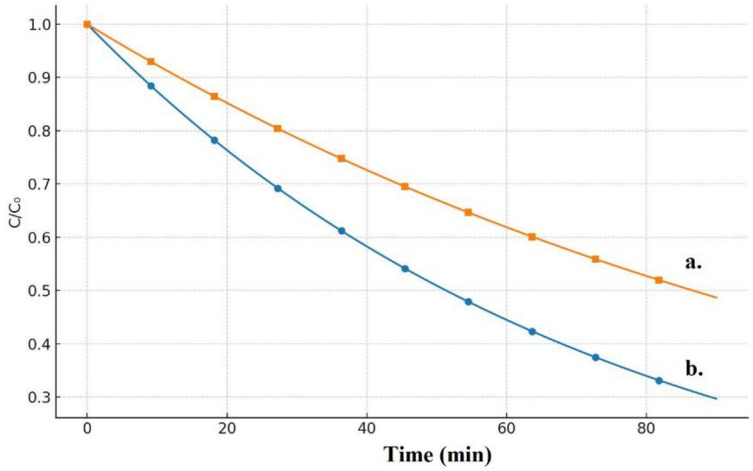

Fig. 4. Plot pseudo-first-order of MB photodegradation a. IO and b. SSIO.

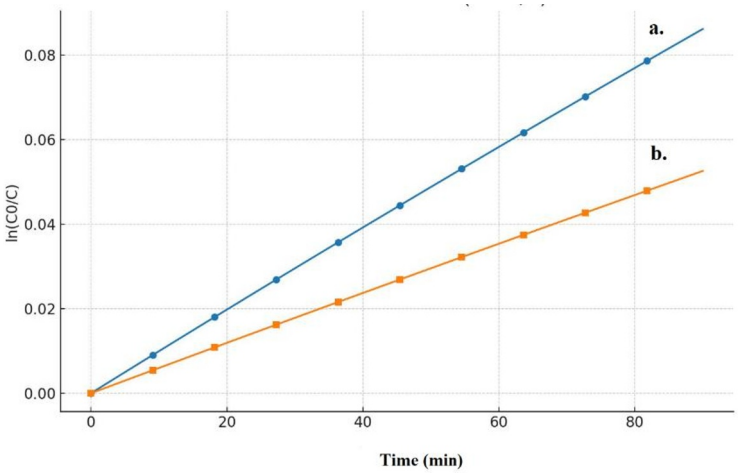

Fig. 5. Plot pseudo-second-order of photodegradation a. SSIO and b. IO.

The kinetic parameters summarized in Table 1 and Figures 4–5 clearly demonstrate that the SSIO catalyst exhibits faster and more efficient photodegradation performance compared to pristine IO. The superior activity of SSIO can be attributed to the abundance of surface –SO_3H and –OH functional groups on the sulfonated silica framework, which not only enhance adsorption of the cationic dye molecules via electrostatic interactions, but also facilitate interfacial charge transfer at the solid–liquid interface. These chemical groups provide additional surface-active sites, which accelerate the formation of reactive oxygen species (ROS) and promote faster decomposition of methylene blue. In line with this surface-enriched functionality, the pseudo-first-order model provided the best correlation for both catalysts, yielding an estimated R^2 value of 0.98 for SSIO and 0.95 for IO, with a higher apparent rate constant obtained for SSIO (0.0135 min^{-1}).

A similar trend is observed under the pseudo-second-order model, where SSIO again exhibits a steeper decline in $\ln(C_0/C)$ (Figure 5), indicating that the functionalized surface accelerates both adsorption and subsequent surface reaction steps. However, the slightly

lower R^2 values obtained for the pseudo-second-order model (0.92 for SSIO and 0.88 for IO) suggest that the photodegradation mechanism is predominantly governed by surface reaction kinetics rather than mass-transfer or diffusion processes. Overall, the enhanced kinetics of SSIO can be directly attributed to the presence of $–SO_3H$ and –OH groups, which significantly improve the adsorption/photocatalytic behaviour of the iron oxide catalyst, providing a more efficient reaction pathway for dye removal.

4 Conclusion

The results clearly demonstrate that incorporating sulfonated silica into iron oxide significantly enhances the photocatalytic degradation of methylene blue. The SSIO catalyst contained finely dispersed Fe_2O_3 crystallites (2.08 nm) embedded in a functionalized silica matrix rich in surface –COOH, Si–OH and Si–O–Si groups, which facilitated both dye adsorption and charge separation processes. Compared with the pristine IO sample, SSIO exhibited a significantly higher degradation efficiency (88.7% vs 72.5% after 90 min) and a higher rate constant (0.0135 min^{-1}), confirming the beneficial role of the sulfonated support. The kinetic evaluation, based on a pseudo-first-order model, further indicates that the degradation process is controlled by surface reactions rather than mass transfer. These findings highlight the potential of SSIO as a low-cost and efficient photocatalyst for the remediation of dye-contaminated wastewaters.

Acknowledgments

The author would like to express their sincere gratitude to Universitas Sebelas Maret (UNS) for the financial support provided under the Research Excellence Grant Scheme (PUTA UNS), with the contract number 369/UN27.22/PT.01.03/2025. This funding has been crucial in enabling the successful completion of this research, and the author greatly appreciates the opportunity to contribute to scientific advancements with the support of this esteemed institution. Special thanks are also extended to the faculty and staff who facilitated this research.

References

1. M. Ulfa and W. Apriliani, “Comparative Study of Soft Template on Gunningite Synthesis for Ibuprofen Adsorption Application,” Indones. J. Chem., vol. 23, no. 2, pp. 438–448, 2023, doi: 10.22146/ijc.79098.
2. A. Safri and A. J. Fletcher, “Effective Carbon/TiO2 Gel for Enhanced Adsorption and Demonstrable Visible Light Driven Photocatalytic Performance,” Gels, vol. 8, no. 4, 2022, doi: 10.3390/gels8040215.
3. W. K. Essa et al., “Polyethylene Terephthalate Nanofiber-Multi-Walled Carbon Nanotube Composite,” Water, vol. 25, 2022.
4. S. Majumder, S. Bhattacharjee, and C. K. Ghosh, “NiO/Ag heterostructure: Enhanced UV emission intensity, exchange interaction and photocatalytic activity,” RSC Adv., vol. 6, no. 61, pp. 56503–56510, 2016, doi: 10.1039/c6ra09432e.
5. A. Gallo, C. Tiozzo, R. Psaro, F. Carniato, and M. Guidotti, “Niobium metallocenes deposited onto mesoporous silica via dry impregnation as catalysts for selective epoxidation of alkenes,” J. Catal., vol. 298, pp. 77–83, 2013, doi: 10.1016/j.jcat.2012.11.015.

6. P. O. Oladoye, M. Kadhom, I. Khan, K. H. Hama Aziz, and Y. A. Alli, “Advancements in adsorption and photodegradation technologies for Rhodamine B dye wastewater treatment: fundamentals, applications, and future directions,” Green Chem. Eng., vol. 5, no. 4, pp. 440–460, 2024, doi: 10.1016/j.gce.2023.12.004.
7. S. D. Frazier and W. V. Srubar, “Evaporation-based method for preparing gelatin foams with aligned tubular pore structures,” Mater. Sci. Eng. C, vol. 62, pp. 467–473, 2016, doi: 10.1016/j.msec.2016.01.074.
8. C. Djama, D. Chebli, A. Bouguettoucha, I. Doudou, and A. Amrane, “Statistical physics modelling of azo dyes biosorption onto modified powder of Acorus calamus in batch reactor,” Biomass Convers. Biorefinery, 2021, doi: 10.1007/s13399-020-01190-2.
9. D. Prasetyoko et al., “Mesoporous ZnO nanoparticles using gelatin - Pluronic F127 as a double colloidal system for methylene blue photodegradation,” vol. 40, no. 1, pp. 112–123, 2023, doi: 10.1007/s11814-022-1224-y.
10. M. Ulfa and I. Setiarini, “The Effect of Zinc Oxide Supported on Gelatin Mesoporous Silica (GSBA-15) on Structural Character and Their Methylene Blue Photodegradation Performance,” Bull. Chem. React. Eng. Catal., vol. 17, no. 2, pp. 363–374, 2022, doi: 10.9767/bcrec.17.2.13712.363-374.
11. M. Nasirian, C. F. Bustillo-Lecompte, and M. Mehrvar, “Photocatalytic efficiency of Fe2O3/TiO2 for the degradation of typical dyes in textile industries: Effects of calcination temperature and UV-assisted thermal synthesis,” J. Environ. Manage., vol. 196, pp. 487–498, 2017, doi: 10.1016/j.jenvman.2017.03.030.
12. M. Ulfa and A. M. Jannah, “Synthesis of Mesoporous Fe 2 O 3 / SBA-15 and its application for Nickel (II) Ion Adsorption,” Orient. J. Chem., vol. 34, no. 1, pp. 420–429, 2018.
13. S. Chatterji, “A discussion of the paper ‘Crystallisation in pores’ by G.W. Scherer,” Cem. Concr. Res., vol. 30, no. 4, pp. 669–671, 2000, doi: 10.1016/s0008-8846(00)00224-6.
14. Z. Luan and J. A. Fournier, “In situ FTIR spectroscopic investigation of active sites and adsorbate interactions in mesoporous aluminosilicate SBA-15 molecular sieves,” Microporous Mesoporous Mater., vol. 79, no. 1–3, pp. 235–240, 2005, doi: 10.1016/j.micromeso.2004.11.012.
15. S. Moein Najafabadi and J. Safaei Ghomi, “Synthesis of COF-SO3H Immobilized on Manganese Ferrite Nanoparticles As An Efficient Nanocomposite in The Preparation of spirooxindoles,” Sci. Rep., vol. 13, no. 1, Dec. 2023, doi: 10.1038/s41598-023-49628-7.